Conformal Hybrid Solar and Electromagnetic (EM) Energy Harvesting Rectenna

Ana Collado, *Senior Member, IEEE*, and Apostolos Georgiadis, *Senior Member, IEEE*

***Abstract*—This paper presents the design of a cost effective, hybrid energy harvesting circuit combining a solar cell and a rectenna capable to harvest ambient electromagnetic energy. Electromagnetic analysis is used to model and optimize the designed circuits in order to allow the antenna and solar cell to share the same area leading to a compact structure. Nonlinear harmonic balance optimization is used to maximize the RF-to-DC conversion efficiency of the rectenna circuitry in the presence of the solar cell and both wideband and multiband topologies are presented. Furthermore, a low cost and flexible polyethylene terephthalate PET substrate and a flexible amorphous silicon solar cell are chosen, providing for both a low cost and conformal structure. A prototype able to generate a maximum DC power of 56 mW when the solar cell is illuminated with $100\ \mathrm{mW/cm^2}$ solar irradiance, and a dual band rectenna demonstrating an efficiency of 15% around 850 MHz and 1850 MHz when illuminated by a microwave signal of $-20\ \mathrm{dBm}$ available power is presented.**

***Index Terms*—Amorphous a:Si-H solar cell, energy harvesting, flexible substrate, harmonic balance, PET, rectenna, solar cell.**

I. Introduction

AMBIENT energy harvesting is receiving significant attention due to the recent interest in implementing low power, energy autonomous sensors. The demand for energy harvesting circuits is fueled by the use of wireless sensor nodes and radio frequency identification (RFID) devices in an increasing number of applications from logistics, and monitoring, to security and healthcare, to name a few [1].

Solar and electromagnetic energy are two of the commonly referred to ambient energy sources, together with kinetic and thermal energy [2]. Solar energy appears as the largest source of ambient energy, provided there is sufficient light. Typical levels of power that solar cells considered in this work can provide are in the order of mW when illuminated using the standard global solar irradiance spectrum corresponding to air mass 1.5 (AM1.5G) [3] and at $\mathrm{T} = 25°$ also known as $1\ \mathrm{sun} = 100\ \mathrm{mW/cm^2}$. This value quickly drops to uW in cloudy conditions or indoor environments. Thin film solar cells such as hydrogenated amorphous silicon a-Si:H solar cells are second generation solar cells able to demonstrate a maximum solar to electric power conversion efficiencies in the order of 10% [4], under 1 sun illumination. The present challenge for third generation solar cells consists of increasing the power conversion efficiency while maintaining a low cost associated with materials and fabrication [5]. In addition to research efforts towards developing low cost and efficient solar cells, significant efforts have focused on low power DC/DC converter systems with maximum power point tracking (MPPT) capability necessary to optimize the performance of solar harvesting systems [6]–[8].

Ambient electromagnetic (EM) power is available in significantly lower levels relative to solar power. Measured results have reported maximum values in the order of $0.1 - 1\ \mathrm{uW/cm^2}$ [9], [10]. On the other hand, the use of EM-to-DC power conversion circuits or rectennas [11] additionally allows for wireless power transmission, the capability to intentionally power a sensor device using a dedicated low cost transmitter [12]. Furthermore, the utilization of electromagnetic energy harvesters is supported by the fact that sensors typically operate in a wireless environment and scenario, which means that they require the use of antennas. These antennas could be used not only for communications purposes but also for EM energy harvesting. As a result, EM energy harvesters have also enjoyed increased interest in the recent years [13].

Due to the limited and variable nature of ambient energy sources, hybrid harvesting systems are needed in order to provide sufficient energy required to power sensor circuitry [14]. The possibility of integrating solar cells with antenna radiators sharing the same area without degrading the solar cell efficiency or the antenna radiation efficiency was initially proposed by [15] for micro-satellites, and subsequently further developed by [16], [17]. Recently, the possibility of implementing conformal circuits was demonstrated by implementing a solar antenna integrating flexible amorphous silicon solar cells and a textile antenna [18]. The interest in energy harvesting circuits provides an additional motivation for implementing flexible, low cost and compact hybrid solar—electromagnetic harvester circuits and this is the object of this work.

Micro-power rectifier circuits based on diode voltage multipliers such as the Greinacher circuit have been extensively investigated in the literature [19], [20]. The presented work instead focuses on the joint nonlinear and electromagnetic optimization of the input matching network and load of a single diode rectifier circuit for low input available power demonstrating dual band and wideband performance and utilizing low cost flexible substrate materials such as PET.

The level of harvested power from EM energy harvesters is in the order of uW. The solar antenna power levels are in the order of mW under full light condition but this value drops quickly

Manuscript received June 03, 2012; revised October 18, 2012; accepted November 18, 2012. Date of publication January 29, 2013; date of current version July 24, 2013. This work was carried out in the framework of COST Action IC0803 (RFCSET). This work was supported in part by the Marie Curie project SWAP, FP7-PEOPLE-2009-IAPP 251557. This paper was recommended by Associate Editor M. Sanduleanu.

The authors are with the Centre Tecnologic de Telecomunicacions de Catalunya (CTTC), Castelldefels 08860, Spain (e-mail: acollado@cttc.es; ageorgiadis@cttc.es).

Color versions of one or more of the figures in this paper are available online at http://ieeexplore.ieee.org.

Digital Object Identifier 10.1109/TCSI.2013.2239154

under cloudy conditions or in indoor environments. Considering these power levels, the targeted application scenario is for systems that require very low operating duty cycles such as sensors for structural monitoring, as well as for future nanowatt technologies where sensors and devices will have very low consumption leading to nanowatt systems. The development of an hybrid solar/EM harvester is justified in applications where the presence of sufficient energy from a single energy source cannot be ensured. Even though this work focuses on low power EM harvesting it could also be used when intentionally transmitted EM signals of higher power (wireless power transmission) are employed.

Preliminary results of this work have been presented in [21] where a dual band solar-rectenna prototype has been demonstrated. The work presented in this paper contains a more detailed analysis of the nonlinear optimization of the flexible rectifier circuit including multiband and wideband designs, additional simulations and measurements of the solar antenna on flexible substrate, as well as measurements of the joint performance of the rectenna and solar cell in the presence of both EM and solar energy.

In Section II the integration of an amorphous silicon flexible solar cell with a broadband monopole antenna on a low cost, flexible polyethylene terephthalate (PET) substrate is presented. In Section III, combined EM and harmonic balance simulation is used to optimize the rectenna efficiency in the presence of the solar cell and broadband and multi-band designs are compared. In Section IV the final design of a flexible hybrid solar rectenna prototype is presented and simulation is compared with measurements.

II. Solar Radiating Element Design

The designed hybrid solar/EM energy harvester is formed by a rectenna element used for EM energy harvesting and a solar cell. The first step consists of designing a broadband antenna with a solar cell integrated on top of the radiating surface. The proposed structure allows for a compact implementation as both the radiating element and the solar cell module share the same area. The antenna is designed and implemented in flexible polyethylene terephthalate (PET) substrate that permits a conformal implementation. Furthermore, the selected solar cell is a flexible thin-film solar cell in order to preserve the flexibility of the hybrid solar/EM harvester.

A. Broadband Antenna Design

The selected antenna topology is a broadband printed monopole antenna fabricated using PET substrate (Akaflex PCL) of 75 μm thickness and with a copper layer of 35 μm. The dielectric permittivity of the substrate is 3.3 and the loss tangent 0.08. In order to overcome fabrication limitations when using microstrip technology, a coplanar waveguide (CPW) implementation is selected. Furthermore, the use of a single conductive layer required by the CPW implementation does not limit the flexibility of the substrate, in contrast to the case of microstrip technology where two metal layers are necessary.

The broadband monopole has a circular base and a centered feed line (Fig. 1). For the selected CPW technology, the input line is designed to present 50 Ohm which led to the middle conductor line to have 4.6 mm width and the gap between the conductor line and the ground planes to be 0.12 mm (Fig. 1). The antenna is optimized using Ansys HFSS software aiming at minimizing its size by eliminating the metal areas where the current distribution is weaker and thus have less effect on the overall antenna impedance and radiation pattern performance. Additionally, the location of a metal line subsequently used as a DC terminal for the solar cell was also optimized in order not to affect the antenna performance (Fig. 1). It was found by EM simulation that the top part of the monopole was the least sensitive location to connect the solar cell DC terminal line.

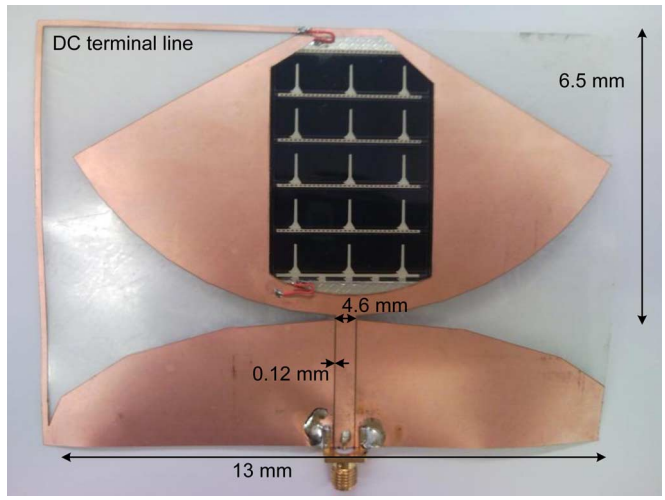

Fig. 1. Photo of the prototype showing the broadband monopole antenna on flexible PET substrate with the solar cell placed on top. One terminal of the solar cell is then connected to the conductor of the monopole antenna and the other terminal to the DC interconnecting line.

The antenna was designed to cover the frequency band extending from 800 MHz to 6 GHz, in order to be suitable for its integration in a variety of EM energy harvesters aiming at different frequency bands corresponding to existing communication standards (GSM-850 MHz, GSM-1900 MHz, ISM 2.45 GHz, ISM 5.8 GHz). The antenna was fabricated using a laser prototyping process in order to etch the PET substrate. Figs. 2(a) and 2(b) show simulations and measurements of the input S-parameters of the designed broadband antenna. One can see that the antenna is matched to 50 Ohms from approximately 800 MHz and extends beyond 6 GHz.

The setup used for measuring the broadband antenna is shown in Fig. 3. The measured radiation patterns of the broadband antenna for selected frequencies (0.85 GHz, 1.85 GHz and 2.45 GHz) are shown in Figs. 4–6. Simulated and measured values of the antenna gain versus frequency are shown in Table I and Fig. 7, where one can see that the measurement curves are slightly shifted to lower frequency values in comparison with the simulated curves.

B. Solar Cell Model and Solar Antenna Design

The selected solar cell is a commercially available flexible hydrogenated amorphous silicon (a-Si:H) solar cell (Fig. 8). The impact that the solar cell has on the antenna is expected to be minimum due to the very small thickness of its material layers as shown in Fig. 8(a). In order to demonstrate this fact, the cell

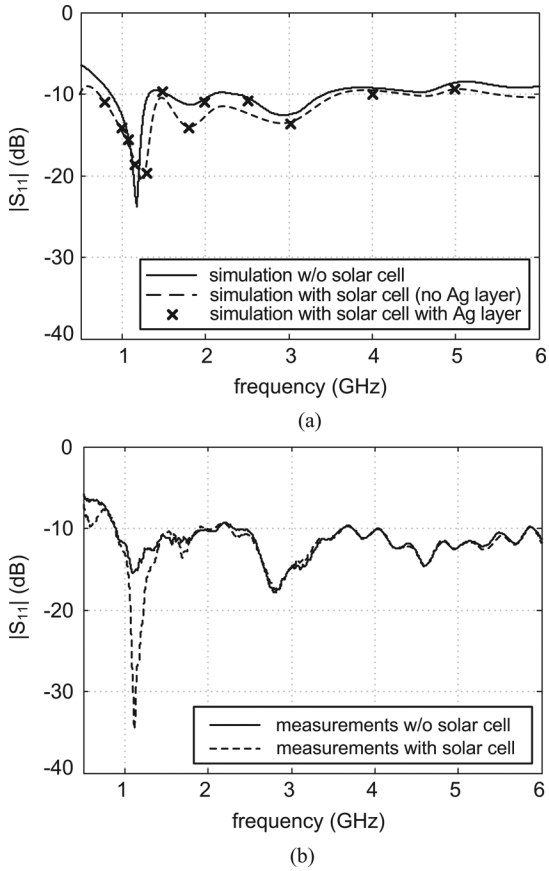

Fig. 2. Input S-parameters of the broadband antenna element (a) Simulated results with and without the integration of the solar cell (b) Measurement results with and without the integration of the solar cell.

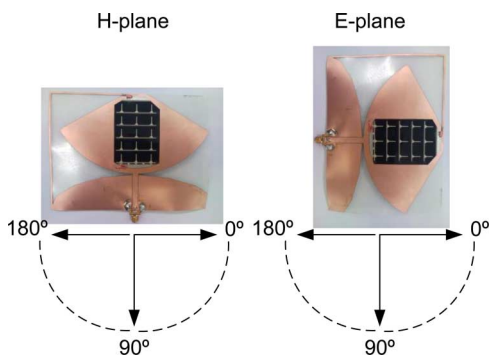

Fig. 3. Set-up used for the measurement of the radiation patterns.

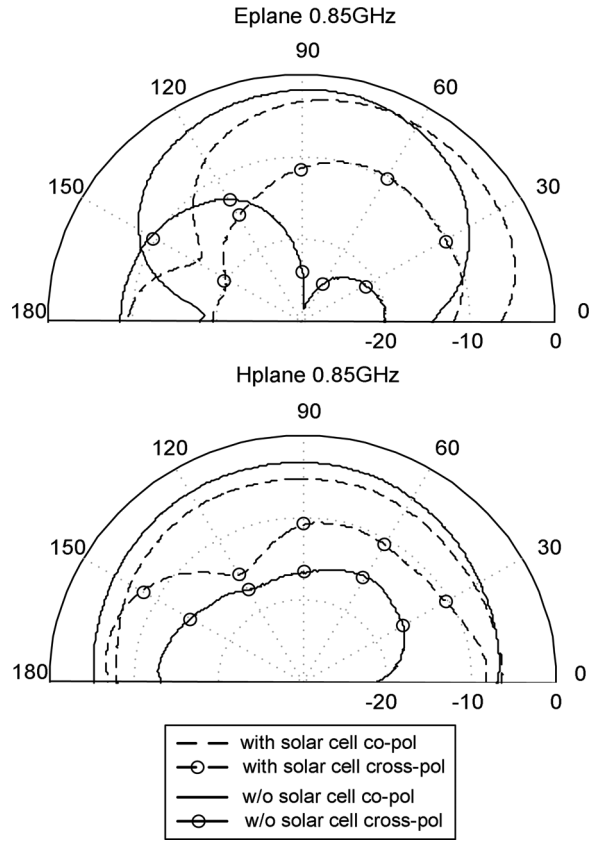

Fig. 4. Measured gain radiation patterns of the broadband antenna with and without the integration of the solar cell for 0.85 GHz.

structure was introduced in Ansys HFSS (Fig. 8(b)). The solar cell layer structure that was used was similar to the one proposed in [17] modified according to the specifications of the purchased cell and can be seen in Fig. 8(a). Light enters the cell through the top transparent conductive layer of ZnO. It then reaches the p-i-n junction where the photo-generation is produced [22]. A reflective back contact formed by a combination of a metal layer (aluminium:Al or silver:Ag) and ZnO is used to obtain high reflectivity properties. The bottom layer corresponds to a flexible layer of polyamide substrate.

In order to minimize the computational load and reduce the simulation time, the only layers considered in the electromagnetic simulation were the substrate polyamide layer because it is the thickest layer in the solar cell structure and the Al layer, as its reflective properties may have a potential impact on the broadband antenna performance. Preliminary simulations including also the Ag layer showed that its effect can be neglected (Fig. 2(a) and Table I).

The current-voltage (I-V) characteristic of the solar cell is measured for the global AM1.5 conditions that assume direct sunlight irradiation of $100\ \mathrm{mW/cm^2}$[5]. The measurements (Fig. 9) show an open circuit voltage of $\mathrm{Voc} = 4.2\ \mathrm{V}$, a short circuit current of $\mathrm{Isc} = 27\ \mathrm{mA}$ and a maximum power point corresponding to $\mathrm{V} = 2.8\ \mathrm{V}$ and $\mathrm{I} = 20\ \mathrm{mA}$ $(\mathrm{P} = 56\mathrm{mW})$.

The selected solar cell was attached to the antenna element using a double-sided glued tape. One terminal of the solar cell is then connected to the conductor of the monopole antenna and the other terminal to the DC terminal line. The simulated and measured input S-parameters of the solar antenna are shown in Figs. 2(a) and 2(b). One can see that the solar cell has little effect on the antenna input impedance. Slight differences in the measured S-parameters of Fig. 2(b) between the antenna and the solar antenna in are attributed to the layer of glue used to stick the solar cell on the surface of the antenna.

The measured radiation patterns of the antenna with and without the solar cell for different frequencies of the antenna band, are shown in Figs. 4–6. One can see that depending on the frequency the solar cell has some effect on the antenna gain, and may also lead to an increase in the cross-polarization levels. The slight shifting of the radiation patterns (Figs. 4–6) of the solar antenna in comparison with the antenna element alone

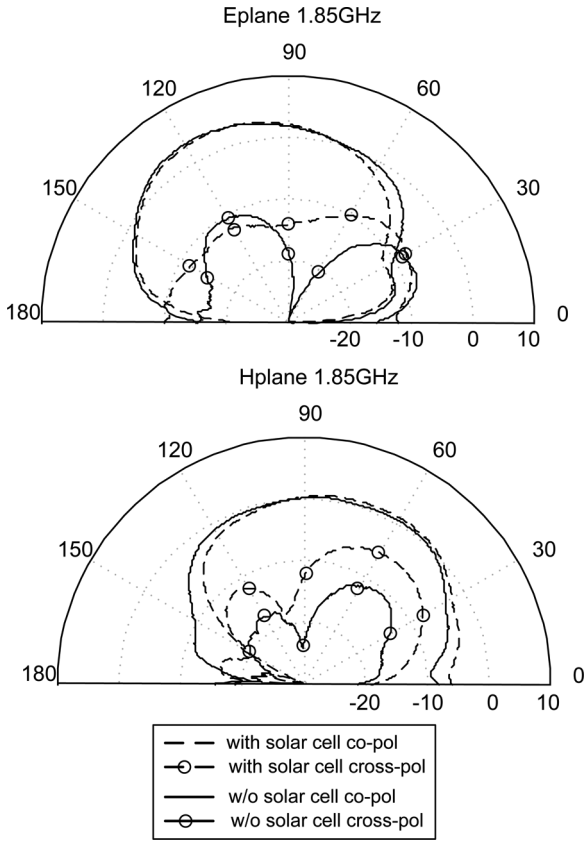

Fig. 5. Measured gain radiation patterns of the broadband antenna with and without the integration of the solar cell for 1.85 GHz.

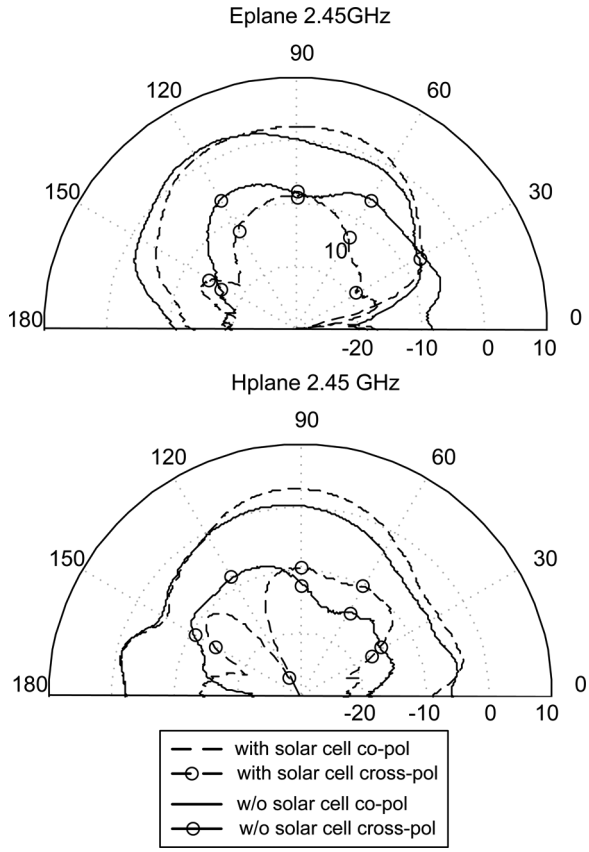

Fig. 6. Measured gain radiation patterns of the broadband antenna with and without the integration of the solar cell for 2.45 GHz.

are attributed to the DC cables connecting the positive and negative terminal of the solar cell to the antenna surface and to the DC interconnection line (Fig. 1). Furthermore, Table I and Fig. 7 show the performance of the broadband antenna in terms of gain with and without the integration of the solar cell. In the considered case a single solar cell was placed on top of the antenna radiating structure. It is also possible to cover the complete area of the radiating structure with solar cells that maybe connected in series or parallel [15]. In order to do so one has to carefully place the adequate diodes to avoid the problem of reverse currents when there is a mismatch either in the current or the voltage values of the different connected solar cells.

III. Optimized Design of Rectifier Circuit

The amount of DC output power that can be obtained from the EM energy harvester directly depends on the RF-to-DC conversion efficiency of the rectifier circuit. It is therefore necessary to maximize the rectifier efficiency at the desired frequencies of operation. Towards this goal it is important to be able to take into account in the optimization setup both the properties of the antenna element that is used to capture the EM signals as well as the matching network placed between the antenna element and the rectifier circuit in order to maximize the transfer of power.

In order to be able to make a joint simulation of the antenna plus rectifier circuit the Thevenin equivalent of the antenna in the receiving mode was used (Fig. 10) [23]. The Thevenin equivalent represents the antenna as an impedance element Z_A

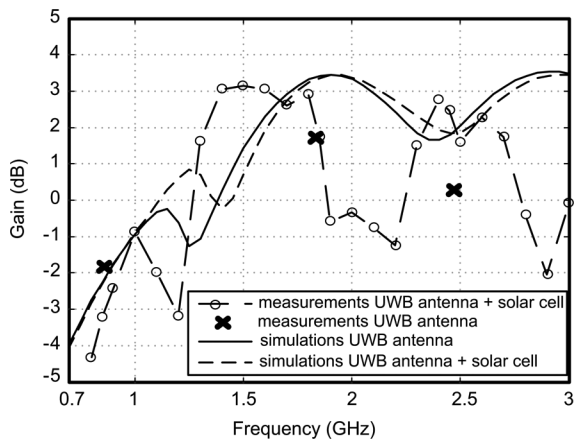

Fig. 7. Broadband monopole antenna gain along the frequency band with and without the integration of the solar cell.

in series with an open circuit voltage source (V_{OC}) which can be calculated using reciprocity theory [24] as

$$V_{oc}(\theta_o, \phi_{o,}, S) = \frac{4\pi}{jk\eta_o}(F\theta_{o,}\phi_{o,})E_o(S) \quad (1)$$

$$E_o(S) = \sqrt{2\eta_o S} \quad (2)$$

where $F(\theta_{o,}\phi_{o,})$ is the far-field electric vector when the antenna is considered in the transmitting mode, assuming a unit current excitation in its port, E_o is the electric field of an incoming plane wave referenced to the center of the antenna, S is the magnitude

TABLE I
ANTENNA GAIN

Freq (GHz)	Simulated Gain w/o Solar cell (dB)	Simulated gain with solar cell as Al layer (dB)	Simulated gain with solar cell as Al+Ag layers (dB)	Measured Gain w/o Solar Cell (dB)	Measured Gain with Solar Cell (dB)
0.85	-2.32	-2.32	-2.33	-1.83	-3.27
1.85	3.35	3.32	3.31	1.84	2.18
2.45	1.65	1.92	1.91	0.24	2.23

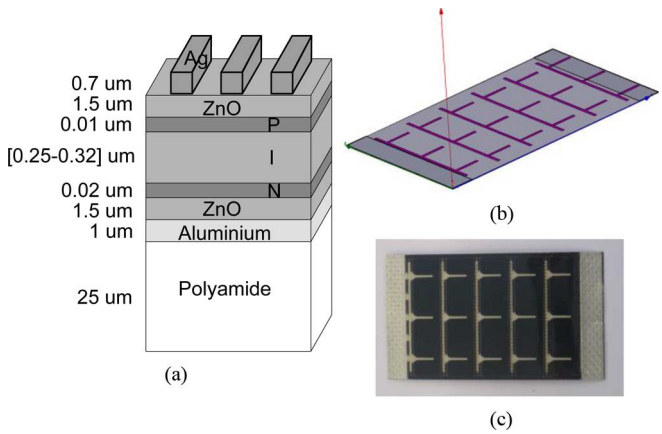

Fig. 8. Solar cell: (a) Model layer structure (b) Ansys HFSS solar cell layout (c) Photo of flexible thin-film solar cell.

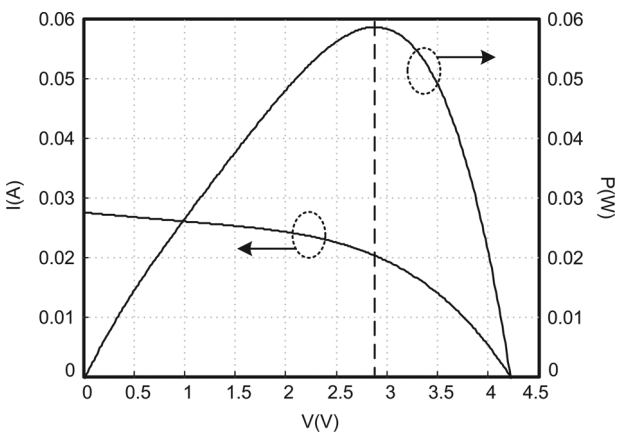

Fig. 9. Measured solar cell I-V characteristic.

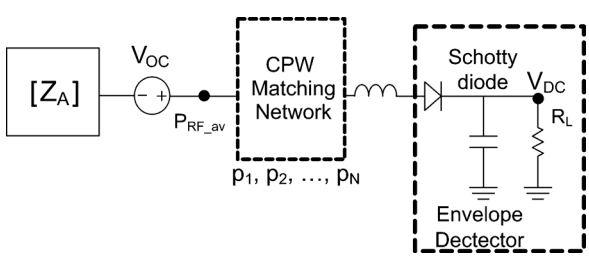

Fig. 10. Schematic used for the joint optimization of the rectenna element.

of the Poynting vector of the plane wave, and $\eta_o = 120\pi$ the wave impedance of free space. Alternatively, a dual formulation based on the Norton equivalent circuit can be used [23].

The above theory was used in [25] to compute the RF-to-DC conversion efficiency of the rectenna as

$$\eta = \frac{P_{DC}}{P_{RF,av}} = \frac{V_{DC}^2}{P_{RF,av} \cdot R_L} \tag{3}$$

$$P_{RF,av} = \frac{|V_{oc}|^2}{8 \cdot Re(Z_A)} \tag{4}$$

where $\mathrm{P_{RF_{av}}}$ is the available RF power, and $\mathrm{Z_A}$ is the complex antenna impedance (Fig. 10) and $\mathrm{Re}()$ indicates real part.

Based on the schematic of Fig. 10, Agilent ADS harmonic balance optimization is used to maximize the RF to DC conversion efficiency $\boldsymbol{\eta}$ in (3), by imposing a suitable goal on its minimum value for the desired frequency range. The optimization parameters are the matching network element values $\mathrm{p_1, p_2, \ldots, p_N}$ (Fig. 10) and the rectifier load $\mathrm{R_L}$ (Fig. 10). By means of an iterative process this minimum value of $\boldsymbol{\eta}_{\min}$ is increased until the optimization process reaches the maximum achievable limit for $\boldsymbol{\eta}$. The impedance Z_A of the antenna element is included in the Agilent ADS simulation using an S-parameter block with the simulation results from Ansys HFSS.

The Skyworks SMS7630 Schottky low barrier diode was used to implement the rectifier circuit. This device presents a low threshold voltage of 135 mV. A simple envelope detector consisting of a series diode and a shunt capacitor was used as it was found that this topology leads to higher conversion efficiency compared to multi-stage diode topologies for low input power levels such as ambient EM power [25]. The efficiency of multi-stage diode rectifiers can be further optimized at low available input power if one is able to control the diode device parameters such as by employing an integrated circuit process [20].

Using the proposed optimization technique, different rectifier structures were designed in order to select the one that leads to an optimum performance of the solar rectenna element. The difference between the designed rectifiers is mainly the selected matching network between the antenna and the rectifying element and the load of the rectifier circuit. The selected available input power level $\mathrm{P_{RF_{av}}}$ assumed in Fig. 10 to optimize the performance of the rectifiers is $-20\ \mathrm{dBm}$.

A. Broadband Rectifier Circuit From 800 MHz to 2.5 GHz

The first rectifier considered is a broadband rectifier that is able to convert incoming EM signals from 800 MHz to 2.5 GHz to DC power. Using the proposed optimization technique the following goal is introduced in the simulation set-up:

$$\eta_{[800\ \mathrm{MHz}-3000\ \mathrm{MHz}]} > \eta_{\min}. \tag{5}$$

In order to fulfill this goal the parameters of the matching network between the antenna and the rectifier circuit are optimized. The resulting network is a dual section stepped impedance broadband network (Fig. 11) that covers the complete frequency band and that presents the adequate impedance to allow the maximum RF-to-DC conversion efficiency. The RF-to-DC conversion efficiency of this design is shown in Fig. 11. The broadband nature of the matching network implies

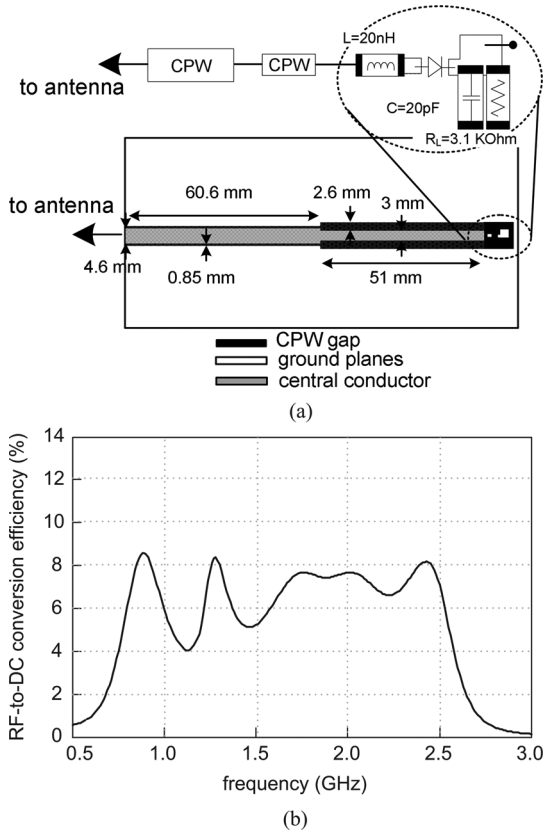

Fig. 11. Broadband rectifier from 800 MHz to 2.5 GHz (a) Schematic of the designed rectifier (b) Simulated RF-to-DC conversion efficiency of the broadband rectifier circuit.

a limit in the minimum achievable magnitude of the reflection coefficient [26]. This limit together with losses associated to the matching network components lead to a reduced RF-to-DC conversion efficiency as can be seen in Fig. 11. The maximum achievable value was around $\boldsymbol{\eta} = 8\%$.

B. Dual-Band Rectifier Circuits

The alternative to achieve higher RF-to-DC conversion efficiency is to design multiband rectifier circuits that have an optimized value of RF-to-DC conversion efficiency at selected smaller frequency bands. Two different dual band designs were done, one for GSM-850 and GSM-1900 and a second one for GSM-850 and ISM band at 2.45 GHz.

The optimized design of the dual band rectifiers requires imposing simultaneously two different goals on the RF-to-DC conversion efficiency (6), one for each of the selected frequency bands

$$\begin{aligned} \eta_{[800\ \mathrm{MHz}-900\ \mathrm{MHz}]} &> \eta_{\min} \\ \eta_{[1800\ \mathrm{MHz}-1900\ \mathrm{MHz}]} &> \eta_{\min} \end{aligned} \tag{6}$$

or

$$\begin{aligned} \eta_{[800\ \mathrm{MHz}-900\ \mathrm{MHz}]} &> \eta_{\min} \\ \eta_{[2400\ \mathrm{MHz}-2500\ \mathrm{MHz}]} &> \eta_{\min}. \end{aligned}$$

TABLE II
MATCHING NETWORK PARAMETERS

Rectifier Design	Lg (nH)	L (nH)	C (pF)	R_L (KOhm)
800 MHz to 2.5 GHz	N/A	20	20	3.1
GSM-850 / GSM-1900	5.6	12	100	2.2
GSM-850 / ISM 2.45GHz	N/A	12	100	2.2

The selected matching network topology for the dual band designs was formed by stepped impedance transmission lines and two short circuit parallel stubs (Fig. 12). Again the values of the matching network parameters are optimized to fulfill the goals in (6) resulting in the CPW matching networks of Fig. 12. The final values of Lg, L, C and $\mathrm{R_L}$ for the three rectifier designs are shown in Table II.

In these two designs the resulting matching networks are dual-band matching networks with improved quality factor with respect to the broadband design which is reflected in an improvement of the RF-to-DC conversion efficiency values. The implemented and measured dual-band rectifier circuits are shown in Fig. 12.

Figs. 13 and 14 show the results of the RF-to-DC conversion efficiency for the two dual-band rectifier circuits. The optimized design of the dual-band rectifier at GSM-850 and GSM-1900 is able to achieve RF-to-DC conversion efficiencies around 15% for both frequency bands (Fig. 13). The dual band rectifier at GSM-850 and ISM 2.45 GHz is able to obtain efficiencies between 10%–12% (Fig. 14). As the measurements of the rectifier circuits were performed using a 50 Ohm signal generator with an available input power of $-20\ \mathrm{dBm}$, the simulation results when substituting the antenna element for a 50 Ohm load have also been included in the figures to facilitate the comparison of the results.

It has to be noted that one of the parameters that highly affects the RF-to-DC conversion efficiency is the output load $\mathrm{R_L}$. There exists an optimum $\mathrm{R_L}$ in order to maximize the efficiency. The evolution of the RF-to-DC conversion efficiency versus $\mathrm{R_L}$ for the dual-band rectifier GSM-850 and GSM-1900 is shown in Fig. 15, where one can see that there exists a value of $\mathrm{R_L}$ that lead to maximum efficiency. It has been shown that the optimum load $\mathrm{R_L}$ does not vary versus the amount of input power at the rectifier [27]. However, it does vary versus frequency [28]. The $\mathrm{R_L}$ value is not the same for 0.85 GHz and 1.85 GHz, so a tradeoff between the maximum efficiency at 0.85 GHz and at 1.85 GHz has to be considered. For this specific rectifier design the selected value of $\mathrm{R_L}$ was 2.2 KOhm. One can see that even though the selected $\mathrm{R_L}$ was the optimum load for 0.85 GHz, the $\boldsymbol{\eta}$ at 1.85 GHz is only reduced by 1% in comparison to its maximum value (Fig. 15).

As stated before the output load of the rectifier $\mathrm{R_L}$ was selected to maximize the conversion efficiency $\boldsymbol{\eta}$ and not to match any specific load corresponding to a desired application. Typically, after the rectifier circuit, one includes a DC/DC converter with input impedance equal to $\mathrm{R_L}$ in order to preserve the obtained conversion efficiency $\boldsymbol{\eta}$ of the rectifier. The output load of the DC/DC converter should match that of the selected device or application.

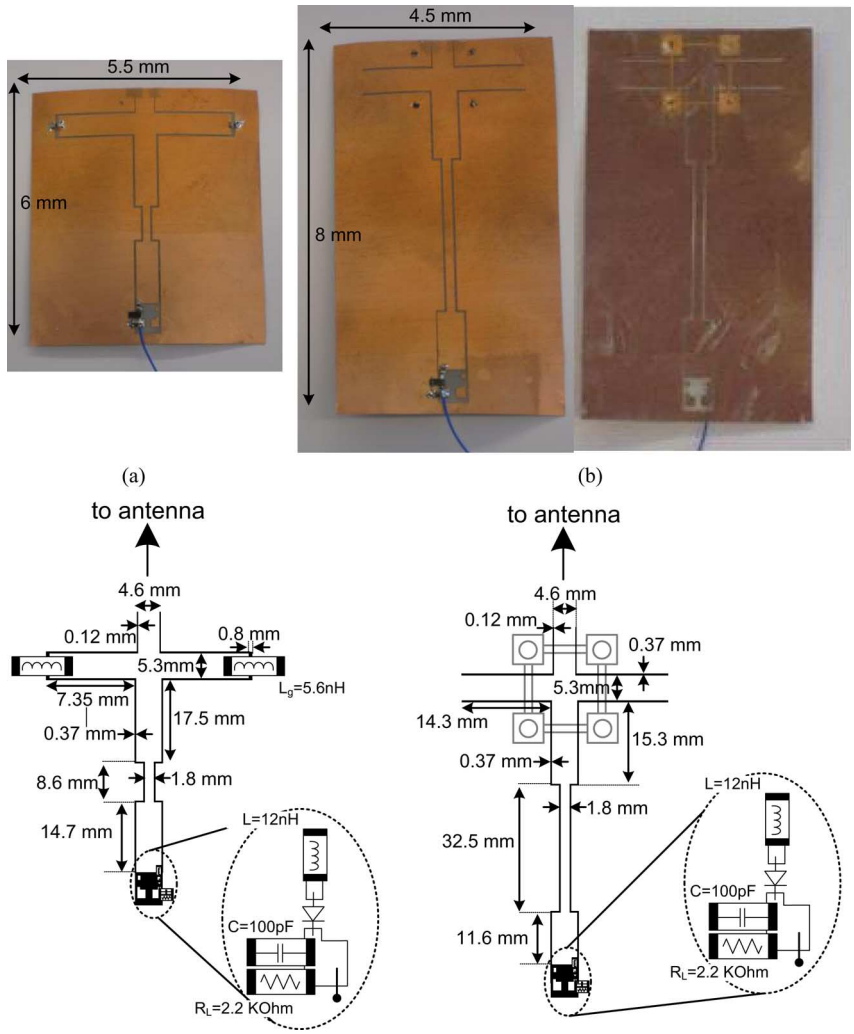

Fig. 12. Implemented dual band rectifiers (a) Dual-band GSM-850 and GSM-1900 rectifier (b) Dual-band GSM-850 and ISM 2.45 GHz rectifier.

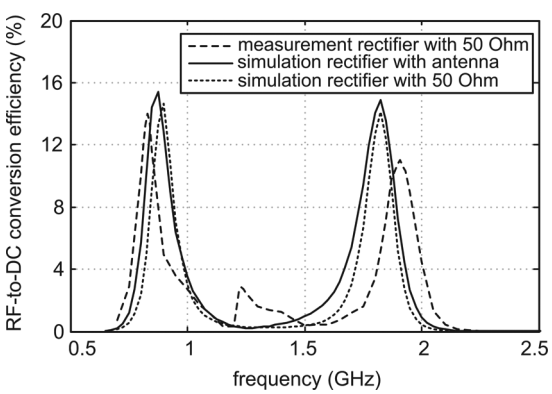

Fig. 13. RF-to-DC conversion efficiency of the dual band rectifier circuit for GSM-850 and GSM-1900 bands versus frequency.

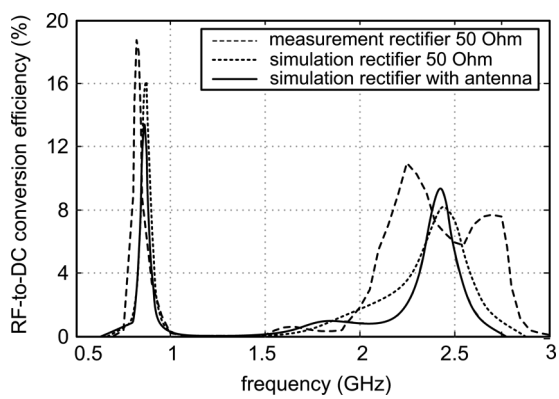

Fig. 14. RF-to-DC conversion efficiency of the dual band rectifier circuit for GSM-850 and ISM-2.45 GHz bands versus frequency.

The results obtained for the previous designs in terms of RF-to-DC conversion efficiency for low input power levels are similar to the ones present in the literature [13], which shows an RF-to-DC conversion efficiency of $< 1\%$ for input power levels $< -17\ \mathrm{dBm}$ at 3 GHz. In Fig. 16 one can see the evolution of the RF-to-DC conversion efficiency for the dual-band rectifier GSM-850 and GSM-1900 for different available input power levels in order to show that for higher input power levels the efficiency increases up to 40%.

IV. Solar Rectenna Performance

In order to implement the final design of the complete solar rectenna system, the design of the dual band rectifier

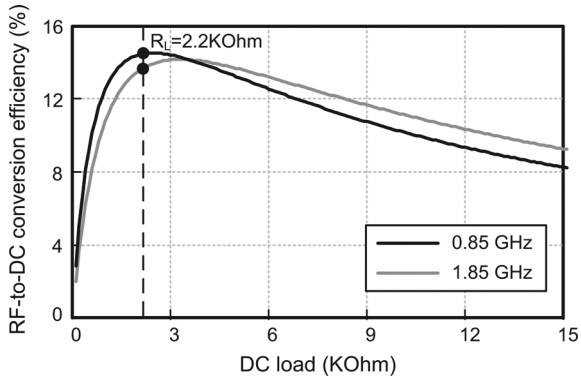

Fig. 15. RF to DC conversion efficiency versus the rectifier load $\mathrm{R_L}$.

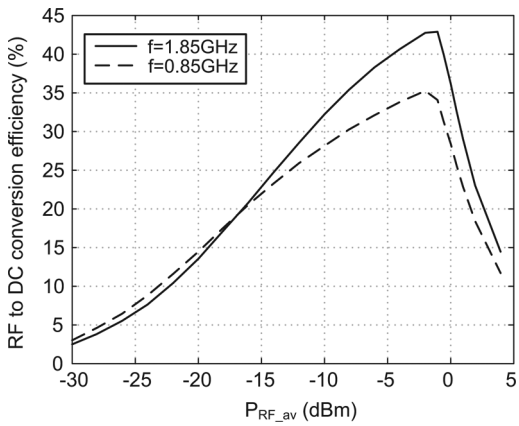

Fig. 16. RF to DC conversion efficiency versus the available power at the input of the rectifier.

at GSM-850 and GSM-1900 was selected as it presents the highest RF-to-DC conversion efficiency of the three presented designs.

The complete solar/EM hybrid energy harvester implemented (Fig. 17) was placed in the anechoic chamber to evaluate the performance of the EM energy harvester with and without the integration of the solar cell. An RF signal was transmitted towards the hybrid harvester from a distance of 3.45 m and the obtained DC voltage at the output of the rectifier circuit was measured. The results obtained with this measurement setup are shown in Fig. 18. The low output voltage is due to the low power density (S) arriving at the rectenna, which results in an available power less than $-20\ \mathrm{dBm}$.

One can see from Fig. 18 that the performance of the EM energy harvester when integrating the solar cell on top is similar to the performance without the solar cell. Another parameter that was considered for this test was the effect of the bending of the structure on the obtained DC voltage. Two different radii of curvature R for the structure were considered $\mathrm{R} = 7\ \mathrm{cm}$ and $\mathrm{R} = 10\ \mathrm{cm}$. The performance of the EM harvester was only slightly affected by the bending of the system showing a robust structure.

Finally, the performance of the simultaneous operation of the rectenna and solar cell was evaluated. In order to have sufficient light to excite the solar cell, an outdoor setup was put together, where a signal generator and an ultra-wideband dipole

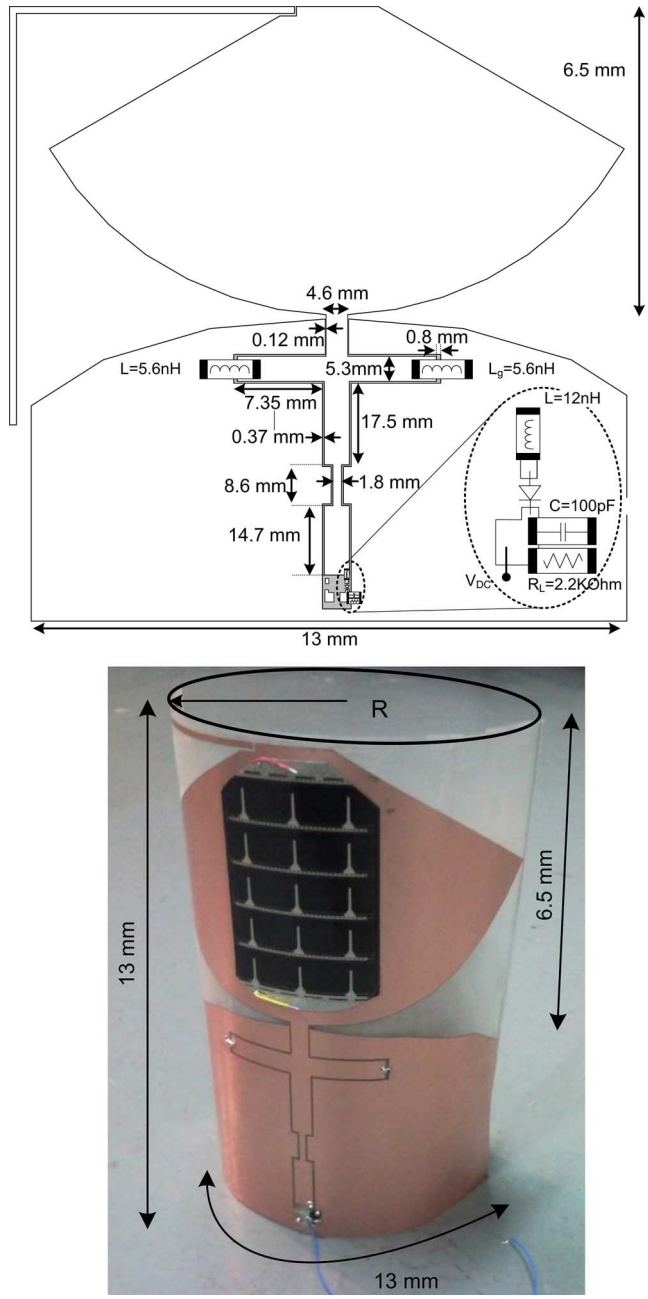

Fig. 17. Hybrid solar/EM energy harvester implementation.

were used to transmit an RF signal to the solar-rectenna from a distance of 70 cm, while the solar cell was illuminated by sunlight. An irradiance value of $99\ \mathrm{mW/cm^2}$ was measured using a solar radiation meter when the solar cell was placed under direct sunlight. It should be noted that the measured irradiance is very close to the 1 sun value $(100\ \mathrm{mW/cm^2})$ typically used to evaluate solar cell performance. Under this illumination condition the solar cell provided an open circuit voltage $\mathrm{Vc} = 4.06\ \mathrm{V}$ and a short circuit current $\mathrm{I_{sc}} = 23.2\ \mathrm{mA}$. A second irradiance measurement of $15\ \mathrm{mW/cm^2}$ was obtained by placing the solar-rectenna in the shade. In this case an open circuit voltage $\mathrm{Vc} = 3.90\ \mathrm{V}$ and a short circuit current $\mathrm{I_{sc}} = 4.3\ \mathrm{mA}$ were measured. The values of open circuit voltage and short circuit

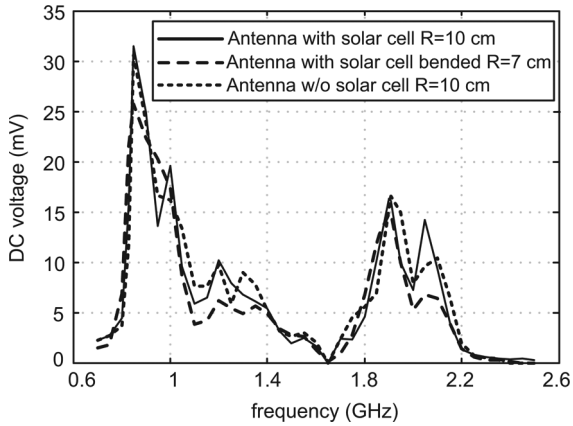

Fig. 18. DC voltage obtained from the EM energy harvester under no solar irradiance. Evaluation of bending on the rectenna performance.

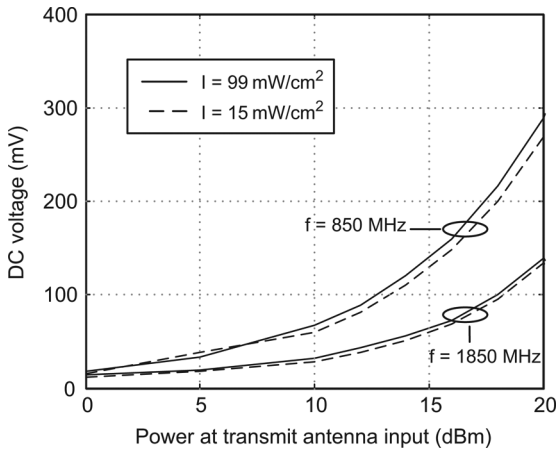

Fig. 19. DC voltage obtained from the EM energy harvester under solar illumination of the solar cell.

current under both irradiation conditions did not show any variation while the available RF power at the rectenna input was varied from $-25\ \mathrm{dBm}$ to $-10\ \mathrm{dBm}$ by adjusting the RF signal generator power from 0 dBm to 20 dBm. The solar cell DC output was not affected by the RF power present at the antenna.

The rectenna DC output was recorded while sweeping the RF signal generator power, for the two solar irradiance conditions mentioned above. The results are shown in Fig. 19 for RF signal frequencies of 850 MHz and 1850 MHz corresponding to the two frequency bands where the rectenna efficiency was optimized. At higher frequency less DC output is obtained due to the larger propagation loss. The slight variation shown in Fig. 19 between the curves corresponding to a different solar irradiance was rather attributed to the effect of the test environment in the transmit antenna and rectenna while setting up the testbed to permit direct sunlight to reach the solar rectenna or placing the rectenna under shade, and not to the difference in solar irradiance.

The solar cell and rectenna circuits shared the same DC ground reference while the output signal from each DC source was recorded separately. It is the object of future work to design an efficient DC power combining circuit and interface circuit forming a complete energy harvesting solution powering a rechargeable battery or super-capacitor.

V. Conclusion

In this paper the optimized design of a conformal hybrid solar/EM energy harvester has been presented. A model for the solar cell used has been proposed and a joint EM simulation of the solar cell and antenna element has been presented. Finally a method to obtain an optimized design of the EM energy harvester that allows a joint simulation of the radiating element and the rectifier circuit using reciprocity theory has been proposed and used to design several rectifier circuits. Final implementation of the optimum hybrid harvester design has been done showing good performance.

Acknowledgment

The authors would like to acknowledge Selva Via for assisting in the fabrication of the circuit prototypes used in this work.

References

[1] R. Vyas, V. Lakafosis, A. Rida, N. Chaisilwattana, S. Travis, J. Pan, and M. M. Tentzeris, "Paper-based RFID-enabled wireless platforms for sensing applications," *IEEE Trans. Microw. Theory Tech.*, vol. 57, no. 5, pp. 1370–1382, May 2009.

[2] S. Beeby and N. White, *Energy Harvesting for Autonomous Systems*. Norwood, CA, USA: Artech House, 2010.

[3] "American Society for Testing and Materials (ASTM) Terrestrial Reference Spectra for Photovoltaic Performance Evaluation," [Online]. Available: http://rredc.nrel.gov/solar/spectra/am1.5/

[4] M. A. Green, K. Emery, Y. Hishikawa, and W. Warta, "Solar cell efficiency tables (version 38)," *Progr. Photovoltaics: Res. Appl.*, vol. 19, pp. 565–572, Aug. 2011.

[5] M. Green, *Third Generation Photovoltaics, Advanced Solar Energy Conversion*. Berlin, Heidelberg: Springer-Verlag, 2006.

[6] C. Alippi and C. Galperti, "An adaptive system for optimal solar energy harvesting in wireless sensor network nodes," *IEEE Trans. Circuits Syst. I, Reg. Papers*, vol. 55, no. 6, pp. 1742–1750, Jul. 2008.

[7] D. Brunelli, C. Moser, L. Thiele, and L. Benini, "Design of a solar-harvesting circuit for batteryless embedded systems," *IEEE Trans. Circuits Syst. I, Reg. Papers*, vol. 56, no. 11, pp. 2519–2528, Nov. 2009.

[8] M. Danesh and J. R. Long, "Photovoltaic antennas for autonomous wireless systems," *IEEE Trans. Circuits and Syst. II, Exp. Briefs*, vol. 58, no. 12, pp. 807–811, Dec. 2011.

[9] H. J. Visser, A. C. F. Reniers, and J. A. C. Theeuwes, "Ambient RF energy scavenging: GSM and WLAN power density measurements," in *Proc. 2008 Eur. Microwave Conf. (EuMC)*, Amsterdam, Netherlands, Oct. 2008, pp. 27–31.

[10] Y. Kawahara, K. Tsukada, and T. Asami, "Feasibility and potential application of power scavenging from environmental RF signals," in *Proc. IEEE Intl. Conf. Antennas Propag. (AP-S)*, Charleston, Jun. 2009, pp. 1–4.

[11] W. C. Brown, R. H. George, and N. I. Heeman, "Microwave to DC converter,"," U.S. Patent 3 434 678, 1969.

[12] W. C. Brown, "The history of power transmission by radio waves," *IEEE Trans. Microw. Theory Tech.*, vol. 32, no. 9, pp. 1230–1242, Sep. 1984.

[13] J. A. Hagerty, F. B. Helmbrecht, W. H. McCalpin, R. Zane, and Z. B. Popovic, "Recycling ambient microwave energy with broadband rectenna arrays," *IEEE Trans. Microw. Theory Tech.*, vol. 52, no. 3, pp. 1014–1024, Mar. 2004.

[14] A. Upson, "Putting wireless to work," *IEEE Spectrum*, pp. 63–63, Jun. 2008.

[15] M. Tanaka, R. Suzuki, Y. Suzuki, and K. Araki, "Microstrip antenna with solar cells for microsatellites," in *Proc. IEEE Int. Symp. Antennas Propagation (AP-S)*, Jun. 20–24, 1994, vol. 2, pp. 786–789.

[16] M. Zawadzki and J. Huang, "Integrated RF antenna and solar array for spacecraft application," in *Proc. 2000 IEEE Int. Conf. Phased Array Syst. Technol., 2000*, Dana Point, CA, May 2000, pp. 239–242.
[17] S. Vaccaro, J. R. Mosig, and P. de Maagt, "Two advanced solar antenna "SOLANT" designs for satellite and terrestrial communications," *IEEE Trans. Antennas Propag.*, vol. 51, no. 8, pp. 2028–2034, Aug. 2003.
[18] F. Declercq, A. Georgiadis, and H. Rogier, "Wearable aperture-coupled shorted solar patch antenna for remote tracking and monitoring applications," in *Proc. 5th Eur. Conf. Antennas Propagation (EUCAP)*, Rome, Italy, Apr. 11–15, 2011, pp. 2992–2996.
[19] J.-P. Curty, N. Joehl, F. Krummenacher, C. Dehollain, and M. J. Declercq, "A model for μ-power rectifier analysis and design," *IEEE Trans. Circuits Syst. I, Reg. Papers*, vol. 52, no. 12, pp. 2771–2779, Dec. 2005.
[20] Y. Jun, K. Wing-Hung, and T. Chi-Ying, "Analysis and design strategy of UHF micro-power CMOS rectifiers for micro-sensor and RFID applications," *IEEE Trans. Circuits Syst. I, Reg. Papers*, vol. 54, no. 1, pp. 153–166, Jan. 2007.
[21] A. Georgiadis, A. Collado, S. Via, and C. Meneses, "Flexible hybrid solar/EM energy harvester for autonomous sensors," in *Proc. 2011 IEEE MTT-S Intl. Microwave Symp. (IMS)*, Baltimore, MD, USA, Jun. 5–10, 2011.
[22] A. V. Shah, H. Schade, M. Vanecek, J. Meier, E. Vallat-Sauvain, N. Wyrsch, U. Kroll, C. Droz, and J. Bailat, "Thin-film silicon solar cell, technology," *Prog. Photovolt: Res. Appl.*, vol. 12, pp. 113–142, 2004.
[23] J. R. Mautz and R. F. Harrington, "Modal analysis of loaded N-port scatterers," *IEEE Trans. Antennas Propag.*, vol. AP-21, no. 2, pp. 188–199, Mar. 1973.
[24] R. E. Collin, *Antennas and Radiowave Propagation*. New York: Mc-Graw-Hill, 1985.
[25] A. Georgiadis, G. Andia-Vera, and A. Collado, "Rectenna design and optimization using reciprocity theory and harmonic balance analysis for electromagnetic (EM) energy harvesting," *IEEE Antennas Wireless Propag. Lett.*, vol. 9, pp. 444–446, 2010.
[26] M. P. David, *Microwave Engineering*, 3rd ed. New York: Wiley, 2004.
[27] T. Paing, J. Shin, R. Zane, and Z. Popovic, "Resistor emulation approach to low-power RF energy harvesting," *IEEE Trans. Power Electronics*, vol. 23, no. 3, pp. 1494–1501, May 2008.
[28] A. Costanzo, M. Fabiani, A. Romani, D. Masotti, and V. Rizzoli, "Co-design of ultra-low power RF/microwave receivers and converters for RFID and energy harvesting applications," in *Proc. IEEE MTT-S Int. Microw. Symp. Digest (MTT)*, May 23–28, 2010, pp. 856–859.

Ana Collado (M'07) was born in Santander, Spain. She received the B.S. degree in telecommunications engineering and the Ph.D. degree from the University of Cantabria, Santander, in 2002 and 2007, respectively.

In 2002, she was with the University of the Basque Country, Bilbao, Spain, studying the uncertainty in the noise figure measurements in monolithic microwave integrated circuit low-noise amplifiers. Since July 2007, she is a Research Associate with the Centre Tecnològic de Telecomunicacions de Catalunya, Castelldefels, Spain, in the area of communication subsystems. Her areas of interest include the development of techniques for practical bifurcation control and stability analysis of power amplifiers and coupled-oscillator systems, and RFID technology and energy harvesting.

Dr. Collado is a 2011 Marie Curie Fellow Researcher for project EU FP7–251557 Symbiotic Wireless Autonomous Powered system (SWAP), and Management Committee Member and Grant Holder Representative of EU COST Action IC0803, RF/Microwave communication subsystems for emerging wireless technologies (RFCSET). She is involved in a number of technical program committees and serves as a reviewer for several journals including IEEE Transactions on Antennas and Propagation, and IEEE TRANSACTIONS ON MICROWAVE THEORY AND TECHNIQUES.

Apostolos Georgiad (S'94–M'03–SM'08) was born in Thessaloniki, Greece. He received the B.S. degree in physics and M.S. degree in telecommunications from the Aristotle University of Thessaloniki, Greece, in 1993 and 1996, respectively. He received the Ph.D. degree in electrical engineering from the University of Massachusetts at Amherst, MA, USA, in 2002.

In 1995, he spent a semester with Radio Antenna Communications (R.A.C.), Milan, Italy, where he was involved with Yagi antennas for UHF applications. In 2000, he spent three months with Telaxis Communications, South Deerfield, MA, USA, where he assisted in the design and testing of a pillbox antenna for LMDS applications. In 2002, he joined Global Communications Devices (GCD), North Andover, MA, USA, where he was a systems engineer involved with CMOS transceivers for wireless network applications. In June 2003, he was with Bermai Inc., Minnetonka, MN, USA, where he was an RF/analog systems architect. In 2005, he joined the University of Cantabria in Santander, Spain, as a researcher. While with the University of Cantabria, he collaborated with Advanced Communications Research and Development, S.A. (ACORDE S.A.), Santander, Spain, in the design of integrated CMOS voltage controlled oscillators (VCOs) for ultrawideband (UWB) applications. Since 2007, he has been a Senior Research Associate at Centre Tecnològic de Telecomunicacions de Catalunya (CTTC), Barcelona, Spain, in the area of communications subsystems where he is involved in active antennas and antenna arrays and more recently with radio-frequency identification (RFID) technology and energy harvesting.

Dr, Georgiadis was the recipient of a 1996 Fulbright Scholarship for graduate studies with the University of Massachusetts at Amherst, the 1997 and 1998 Outstanding Teaching Assistant Award presented by the University of Massachusetts at Amherst, MA, USA, 1999, 2000 Eugene M. Isenberg Award presented by the Isenberg School of Management, University of Massachusetts at Amherst, and the 2004 Juan de la Cierva Fellowship presented by the Spanish Ministry of Education and Science. He presently serves at the Editorial board of the Radioengineering Journal and as an Associate Editor of the IET Microwaves Antennas and Propagation Journal and IEEE MICROWAVE AND WIRELESS COMPONENTS LETTERS. He was the Chair of the IEEE RFID Technologies and Applications 2011 (RFID-TA) Conference and the Chair of the IEEE MTT-S International Microwave Workshop Series (IMWS 2011) on "Millimeter Wave Integration Technologies." He was the co-recipient of the EUCAP 2010 Best Student Paper Award and the ACES 2010 2nd Best Student Paper Award. He was the Chairman of EU COST Action IC0803, RF/Microwave communication subsystems for emerging wireless technologies (RFCSET). He is the Coordinator of Marie Curie Industry-Academia Pathways and Partnerships project EU FP7–251557 Symbiotic Wireless Autonomous Powered system (SWAP).